

# HYDROGEN DETECTION BY THIN-FILM PALLADIUM BASED FABRY PEROT SENSORS

By

Yu Yan

Senior Thesis in Electrical Engineering

University of Illinois at Urbana-Champaign

Advisor: Professor Lynford Goddard

April 2014

## Abstract

Thin-film Fabry-Perot hydrogen sensors with various thicknesses of Palladium are simulated, optimized, fabricated and tested. A reflection-transmission setup is built along with the necessary gas flow system. Detectors and thermistors are employed to measure the reflection and transmission of the sensor and the temperature of the system, respectively. Calibration is automated. The spectrum is recorded before and after hydrogen exposure and the change in reflection at the most sensitive wavelength is monitored closely. We extract important information like the limit of detection (minimum concentration detected) and the response time of the sensors we built. We optimize the wavelength used and the calibration process to achieve the most accurate results.

Subject Keywords: hydrogen sensors; palladium based sensors;

## Acknowledgments

I would like to thank Prof. Goddard for advising me for three years of my undergraduate career. His high expectations and focus on professionalism have improved me greatly over the years. I would also like to thank the graduate students Ben Griffin and Steve McKeown for their guidance and direct help in this project. Finally, I thank Manan Raval and Nikhil Sancheti who worked closely with me as undergraduates in this project.

## Contents

1. Introduction.....	1
2. Literature Review.....	3
3. Description of Research Results .....	5
4. Conclusion .....	20
References.....	21

## 1. Introduction

Hydrogen ( $H_2$ ) gas has long been explored as an alternative to fossil fuel due to its abundance in the universe and its cleanliness [1]. However, as it is combustible above 4% concentration,  $H_2$  is also dangerous to use [1]. Therefore, reliable detection of  $H_2$  is crucial for its applications.  $H_2$  also happens to have a weak optical absorption spectrum [2] which necessitates a secondary material if optical sensing is desired.

Palladium (Pd) is a commonly used material for  $H_2$  detection. When Pd is exposed to  $H_2$ , it dissociates  $H_2$  into H atoms that occupy its interstitial sites [2]. This forms a  $PdH_x$  material, where x depends on the partial pressure surrounding the Pd sample [3]. This process results in a change in the complex refractive index of the Pd sample, allowing for optical  $H_2$  detection.

In order to have an objective measurement of the performance of our sensors, we quote the following 15 requirements from [4]:

- indication of hydrogen in concentration range 0.01–10% (safety) or 1–100% (fuel cells)
- safe performance, i.e. explosion proof sensor design and protective housing
- reliable results of sufficient accuracy and sensitivity (uncertainty <5–10% of signal)
- stable signal with low noise
- robustness including low sensitivity to environmental parameters such as:
  - temperature (–30–80 °C (safety), 70–150 °C (fuel cells))
  - pressure (80–110 kPa)
  - relative humidity (10–98%)
  - gas flow rate
- fast response and recovery time (<1 s)
- low cross sensitivity (e.g. hydrocarbons, CO, H<sub>2</sub>S)
- long life time (>5 years)
- low power consumption (<100 mW)
- low cost (<\$100 per system)
- small size
- simple operation and maintenance with long service interval
- simple system integration and interface

By construction, the sensors that we build have the following three advantages:

- low power consumption compared with electrical sensors
- low cost attributed to the following:
  - Pd is less expensive than Platinum (Pt), which is the other material commonly used for H<sub>2</sub> detection.
  - Thin-film Fabry-Perot structured sensors are simple to fabricate.
  - There is a potential for cheap broadband light sources (such as natural sunlight) to be used.
- small size because our sensors are thin-film

This project is an attempt to address some of the other points in the requirement above. The following is a summary of the main results:

- We have broadened the detection range of our sensors by pushing the lower limit of detection to around 0.01% H<sub>2</sub> in N<sub>2</sub>.
- We have reduced thermal, electrical and optical noise so as to have an overall noise in the measured reflectivity of less than 0.07%.
- We have effectively monitored our samples' sensitivity to thermal fluctuations.
- We have automated the calibration and measurement processes.

This thesis will begin with a brief review of the past work done on this topic in Chapter 2, before going into the details of the experimental setup and results in Chapter 3. Finally, we will conclude in Chapter 4 with an overall look at the accomplishments of this project and make suggestions for future work.

## 2. Literature Review

The literature review will be a discussion of other sensors in the context of the following specs:

- Limit of detection
- Response time
- Recoverability

### 2.1 Limit of detection

The lowest limit of detection that I found was published in [5]. The sensor was a heterojunction field-effect transistor (HFET) that operated at 800 °C. It has a low limit of detection of 10ppb (parts per billion).

### 2.2 Response Time

The lowest response time that I found was published in [6]. The sensor was a Pd ultrathin film and is similar to our optical sensor in that a thin film is used; however a change in resistivity is used for their measurements instead of a change in refractive index. It was capable of a response time of 70 ms at 2% H<sub>2</sub>.

### 2.3 Recoverability

Recoverability of an optical H<sub>2</sub> sensor in this thesis refers to the ability of its reflectivity after H<sub>2</sub> exposure to return to its pre-H<sub>2</sub> exposure value. A known hindrance to this process is the phase change of Pd samples upon introduction of H<sub>2</sub> gas as discussed in [2].

As discussed in the introduction, PdH results from an exposure of Pd to H<sub>2</sub>. PdH exists in 2 phases,  $\alpha$  and  $\beta$ , where the  $\alpha$  phase is associated with low concentrations while the  $\beta$  phase is associated with high concentrations. At intermediate concentrations, a mixture of  $\alpha$  and  $\beta$  phase can coexist.

When one says that Pd can recover its optical properties after a purge from H<sub>2</sub>, we need to keep in mind that we are referring to the  $\alpha$  phase. Beyond the  $\alpha$  phase, the Pd lattice is deformed permanently and

a perfect recovery is no longer possible. Depending on film structure and quality, the transition from  $\alpha$  to  $\beta$  phase occurs from 0.1-2%. Since concentration range of general interest is usually greater than 0.1-2%, a solution to this problem needs to be found.

Work published in [7] suggested that annealing resulted in a stabilization of the microstructure, enhanced sensing stability, reliability and durability of H<sub>2</sub> sensors. For our project, we test the impact of annealing of our Pd sensors, particularly its impact on recoverability.

### 3. Description of Research Results

#### 3.1 Experimental Setup

This section describes the experimental setup employed in this project. The basic units of our experimental apparatus are the following:

- Gas Flow Setup
- Temperature Control Setup
- Sensor Fabrication
- Reflection and Transmission Setup
  - o Calibration Setup
  - o Measurement Setup

##### 3.1.1 Gas Flow Setup

A basic schematic of the gas flow setup is shown in Figure 1:

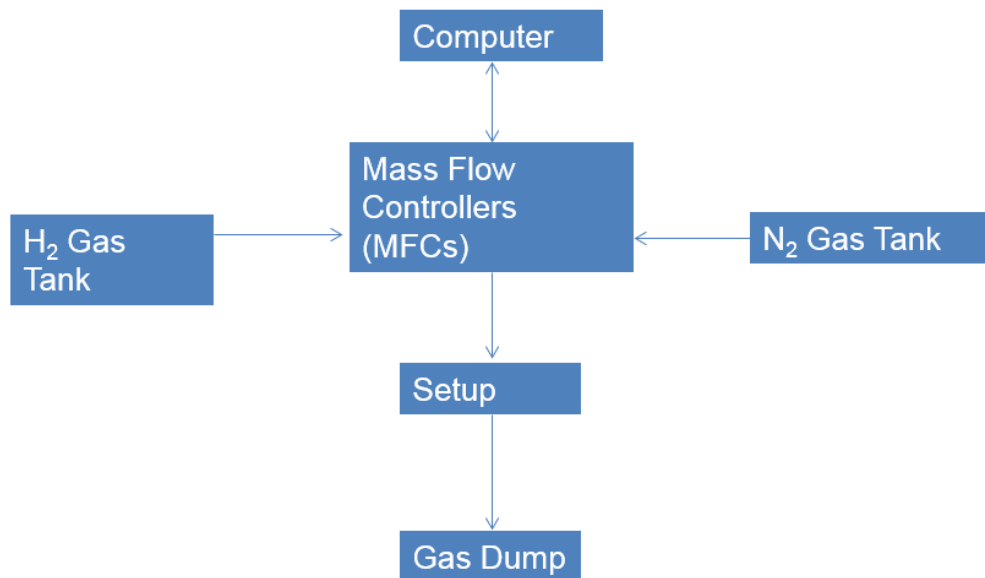


Figure 1

As H<sub>2</sub> is a potentially dangerous gas at concentrations above 4%, we use N<sub>2</sub> gas to dilute the H<sub>2</sub> concentration in our setup. Since we have access to two different gas tanks of pure H<sub>2</sub> and diluted 5% H<sub>2</sub>, and they are both connected to the 4 sccm and 500 sccm mass flow controllers (MFC), and we have control over the N<sub>2</sub> flow rate via the N<sub>2</sub> MFC, we can tune the concentration in our reflection transmission (RT) setup by some simple calculations.

According to the manuals [8-9] (page 4-20 on Sierra manual, page 3 on UNIT manual and page 13 on SEC manual), the Sierra, UNIT and SEC MFC's all have an error of 1% of full scale at any given set point. This means an error of 5 sccm for the 500sccm MFC, 0.04sccm for the 4sccm MFC and 100sccm for the 10000sccm MFC. Thus, we can compute the percent error as a function of set point graph shown on Figure 2.

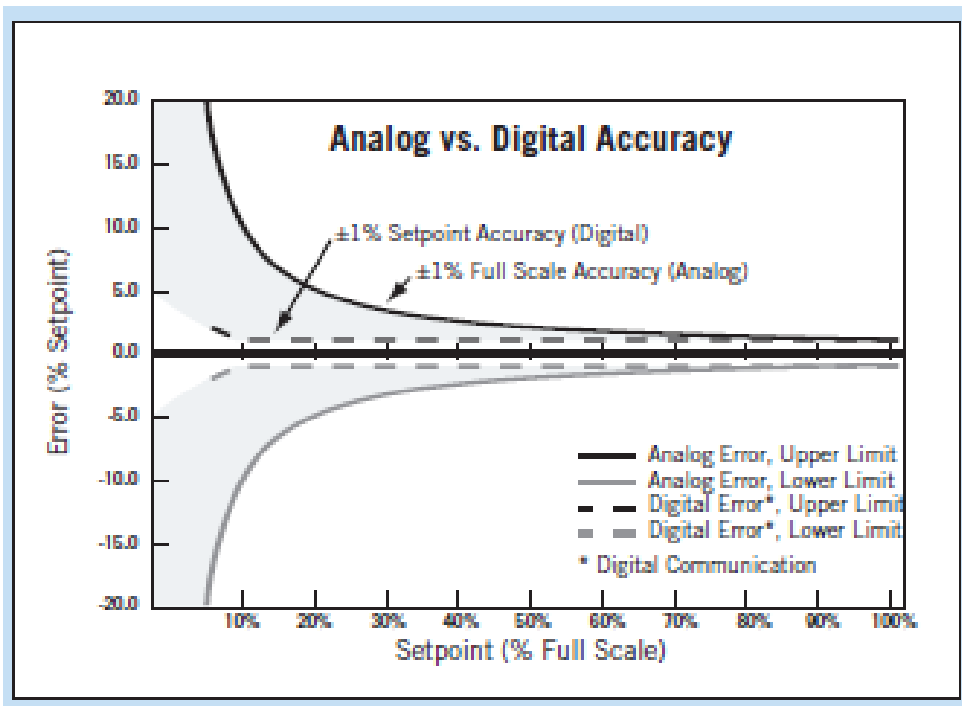


Figure 2 – from [8]

All of the MFCs also have a minimum flow rate of 2% of full scale [8-9]. This translates to 10sccm for a 500sccm MFC, 0.08sccm for a 4sccm MFC and 200sccm for the 10000sccm MFC. Many experts (engineers from the MFC companies) warn against flowing at or near the minimum due to the

larger percentage of error in the achieved set point. They instead recommend using an MFC with a smaller full scale limit.

A more detailed description of the gas flow configuration is shown in Figure 3

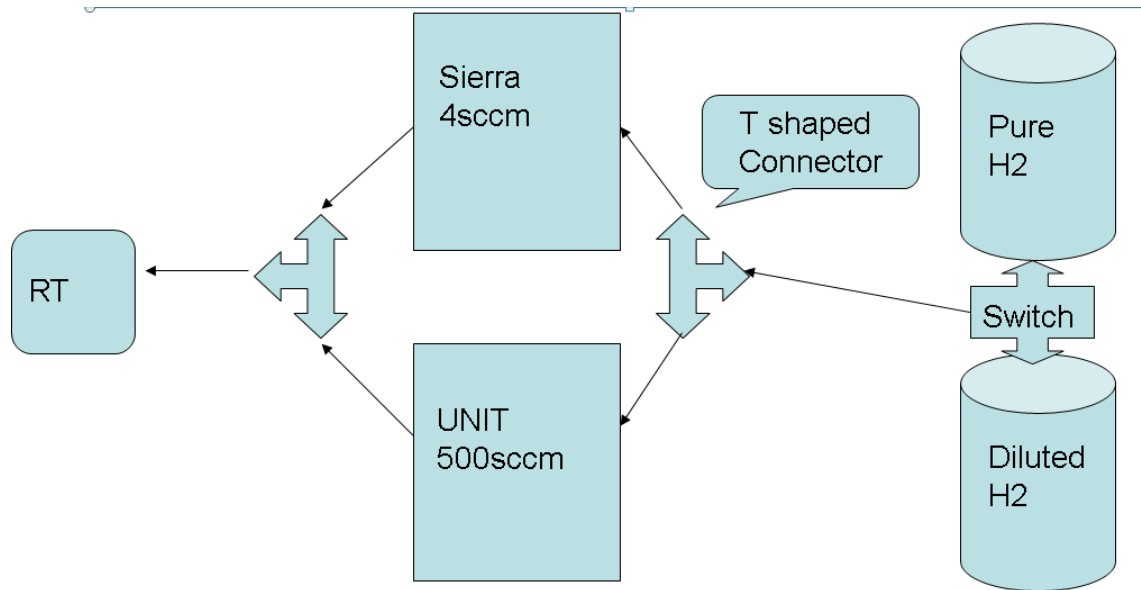


Figure 3

Given our available tanks and MFCs, we have the following possible tank and MFC configurations:

- Pure H<sub>2</sub> + 500sccm MFC
- Pure H<sub>2</sub> + 4sccm MFC
- Diluted H<sub>2</sub> + 500sccm MFC
- Diluted H<sub>2</sub> + 4sccm MFC
- Pure N<sub>2</sub> + 10000sccm MFC

We design our setup assuming that 10% is the maximum acceptable error. For the 10000sccm MFC for pure N<sub>2</sub>, 1000sccm is the 10% error point. We like to constrain the maximum N<sub>2</sub> flow rate to be under 5000sccm to prevent film delamination and other issues.

After a series of calculations which optimizes both the flow range and flow accuracy, we have decided that the following configurations resulted in the desired flow ranges:

- 4sccm MFC for diluted H<sub>2</sub> + 4500sccm N<sub>2</sub> for the ultra-low concentrations (5 to 50 ppm)
- 4sccm MFC for pure H<sub>2</sub> + 4500sccm N<sub>2</sub> for the low concentrations (100 to 1000 ppm)
- 500sccm MFC for diluted H<sub>2</sub> + 4500sccm N<sub>2</sub> for the low concentrations (0.05% to 0.5%)
- 500sccm MFC for pure H<sub>2</sub> + 4500sccm N<sub>2</sub> for the high concentrations (1% to 10%)

### 3.1.2 Temperature Control Setup

Temperature control is done by a feedback process summarized in the schematic shown in Figure 4:

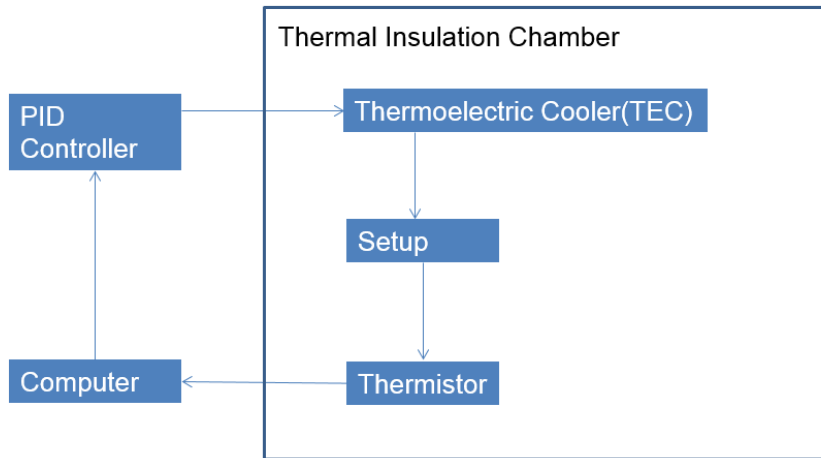


Figure 4

There are two ways in which temperature is controlled in this project. Since the thermal insulation chamber has a strong insulation capability, it is possible to wait for the reflection transmission setup to approach steady state naturally, without any external manipulation of the temperature within. This process takes 5-10 hours on average.

The other way, which has not yet been perfected, is to employ feedback control. With the availability of the components, we already have the capability of tuning the temperature inside the chamber. For example, the TEC components can be manipulated to generate heat inside the chamber. We can then monitor the temperature within the chamber by our thermistor (which sends data directly into the computer). The computer can then act as a controller to manipulate the temperature of the chamber. The problem with this approach is that the TECs work by differential heating and thus require a cooling plate. With the cooling plate in place, heat is transferred between the setup and the room through the bottom optical breadboard plate. Therefore, tuning the temperature with the TECs is a tricky process.

Alternatively, an independent and isolated heating element can be installed inside the system. With such an element, we can move on to thermally isolate the setup from the optical breadboard, or to thermally separate the breadboard and the table. This would result in a completely isolated setup. This heating element should ideally be controllable by the computer, and should have both heating and cooling capabilities (required for PID control). After that, we can implement PID control in the computer and control the temperature directly. This process is much more robust than our current setup and should be able to solve the temperature dependence problem.

### **3.1.3 Reflection Transmission Setup**

The basic schematic of the reflection transmission (RT) setup is shown in Figure 5:

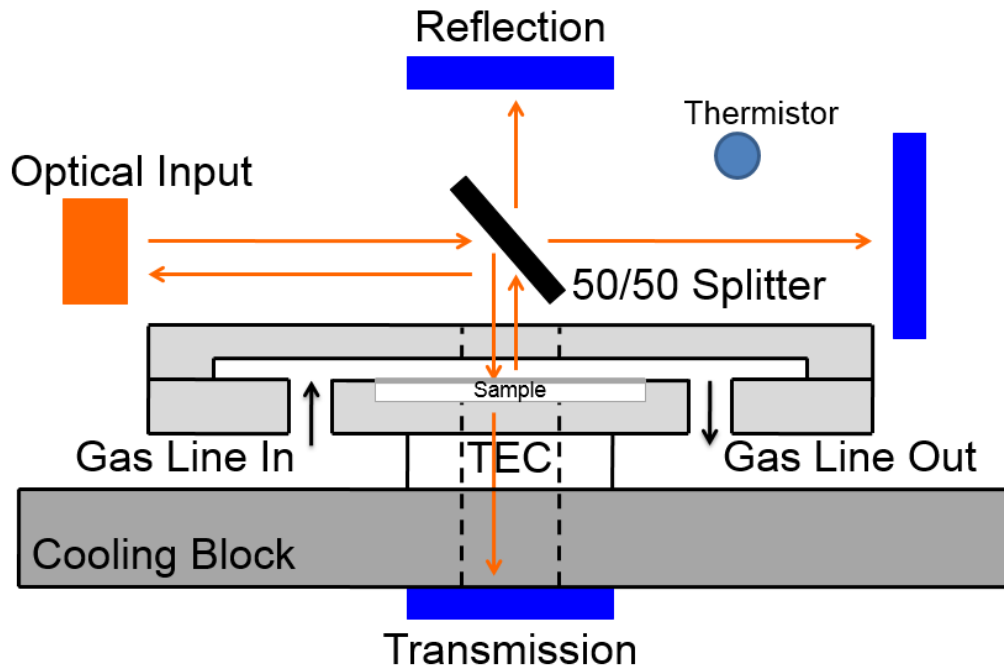


Figure 5

Light enters the setup from the optical input as one of three sources:

- Light emitting diode (LED)
- Broadband lamp
- Tunable laser

It is then sent through a 50/50 beam splitter (Thorlabs model no. BPD254-G), where it is diverted downward through the sample, before entering the transmission photodetector (PD). The PD is Thorlabs model no. PDA50B and is sensitive to 800-1800 nm. Since the sample is a Fabry-Perot cavity (see 3.1.5 for details), part of the light from the sample is reflected back through the splitter and enters into the reflection PD.

Part of the light coming out of the 50/50 beam splitter enters the input PD for the purpose of calibration and normalization.

LabVIEW codes were written with the ability to automatically calibrate the system, yielding key values, e.g. the exact splitting ratio of the beamsplitter. During measurements, these values are loaded in and the measured raw values of reflection, transmission and input power are normalized automatically according to a derived set of equations (not presented in this thesis for brevity). In addition, we have written software codes that are capable of recording the reflection and transmission spectra of our sensors as well as monitoring the reflection and transmission values of single wavelength measurements.

### 3.1.4 Multiple Wavelength Setup

A schematic of the multiple wavelength setup is shown in Figure 6.

An electric motor is used to drive a wheel which contains four filters whose center wavelengths are 850, 1000, 1300, and 1550 nm. The bandwidth of each filter is around 50 nm. In the experiment, the filter wheel will be spinning continuously and the wavelength of light that reaches the photodetector at the output will vary in time. Since the filter wheel is spinning at a relatively fast rate, we are actually monitoring four wavelengths at the same time, hence the name “multiple wavelength”. Code was written that could automatically identify which filter the light had come through based on the recorded oscilloscope waveform and the presence of a narrow slit on the wheel that served as a trigger signal.

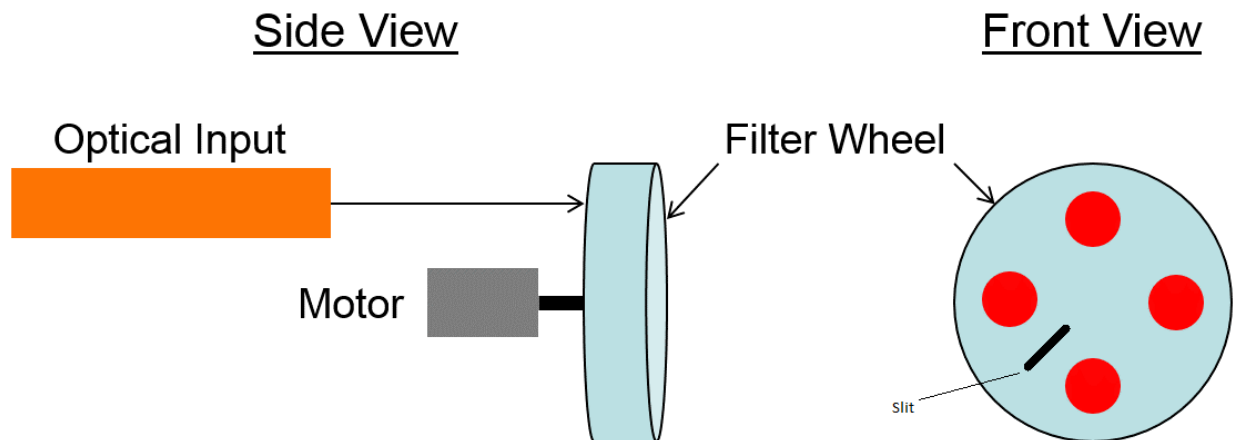


Figure 6

### 3.1.5 Sensor Fabrication

A schematic of a typical sensor is shown in Figure 7.

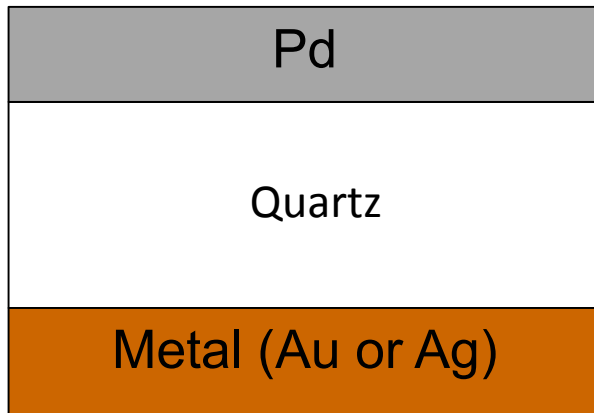


Figure 7

Starting with a quartz substrate, Pd is typically deposited on one side while another metal (typically Au or Ag) are deposited on the other side by an e-beam evaporator. This configuration forms a Fabry-Perot cavity where resonance effects can take place. The typical sensors use 9 nm of Pd and 50 nm of Au on a 1.5 mm thick quartz substrate.

### 3.2 Experimental Results

This section describes the experimental results in this project. They will be discussed in the following order:

- Typical Reflection Spectrum
- Higher Sensitivity at Higher Wavelengths
- Limit of Detection
- Response Times
- Effects of Annealing
- Other Observations

### 3.2.1 Typical Reflection Spectrum

Figure 8 shows a typical reflection spectrum.

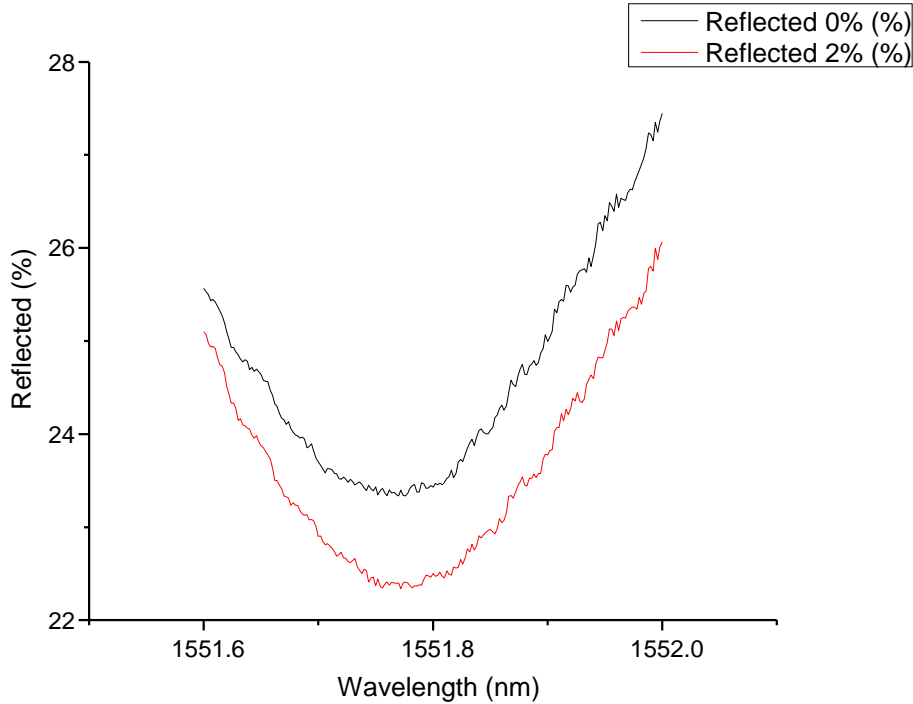


Figure 8

The first observation is that our Pd sensors do respond to  $H_2$  significantly. The maximum change in the reflection spectrum of about 1% amounts to a fractional change of the reflectivity of about 5%. This is a significant and easily measurable response.

The second observation is that the Fabry-Perot structure was indeed successful in creating a spectrum with increased response to  $H_2$  gas in comparison to a plain film.

The third observation is that our speculation earlier that the biggest fractional response occurs at the spectrum minimum was indeed justified. As can be seen in Figure 8, the wavelength of maximum absolute percentage change is the wavelength with the lowest reflection. This adds up to the largest fractional change of 5%.

### 3.2.2 Higher Sensitivity at Higher Wavelengths

The motor wheel described in section 3.1.4 was employed in an experiment which determined the change in sensitivity of our samples with an increase in wavelength. The results are shown in Figure 9.

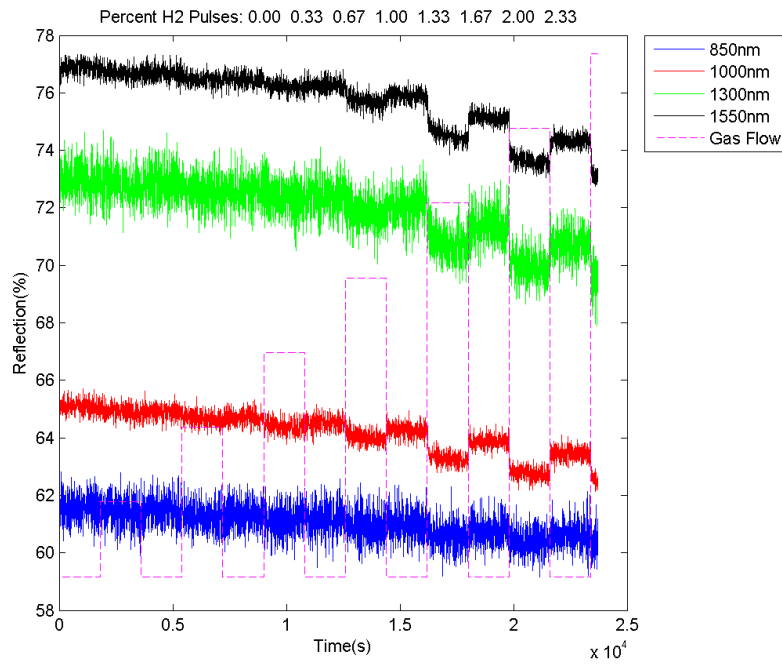


Figure 9

The first observation is that the reflection increases with increasing wavelength.

The second observation is that with increasing wavelength, the absolute change in reflection increases upon introduction of H<sub>2</sub>.

### 3.2.3 Limit of Detection

A limit of detection test was done to find out the lower limit of H<sub>2</sub> gas concentration that our sensors can detect. The results are shown in Figure 10. The numbers under each peak corresponds to the percentage of H<sub>2</sub>.

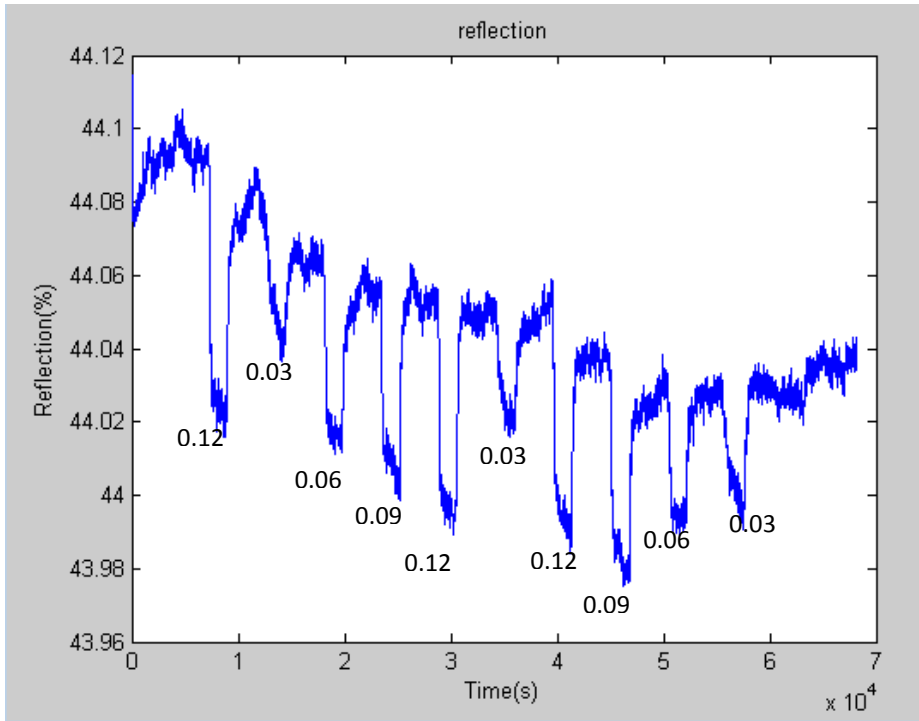


Figure 10

The first observation is that our sensors are clearly responsive at 0.03%. No lower concentrations can be tested due to the constraints placed by our gas flow systems as described in section 3.1.1.

The second observation is that over the period of 70000 s or approximately 19.5 hours, there is a drift in the baseline (the line which the reflection recovers to upon H<sub>2</sub> purge). This is attributed to the drift in temperature in the room. Since the drift happens over a relatively long period of time and its effects are relatively insignificant for any one gas pulse, no measures were taken to address it. If one were interested

in this problem, it is possible to correct the baseline after obtaining the results by using the collected temperature data from the thermistor.

### 3.2.4 Response Times

A 1550 nm light source was used to monitor the response of our sensor to 2% H<sub>2</sub>. Here, the experimental data is used to obtain the response time data. The results are shown in Figure 11.

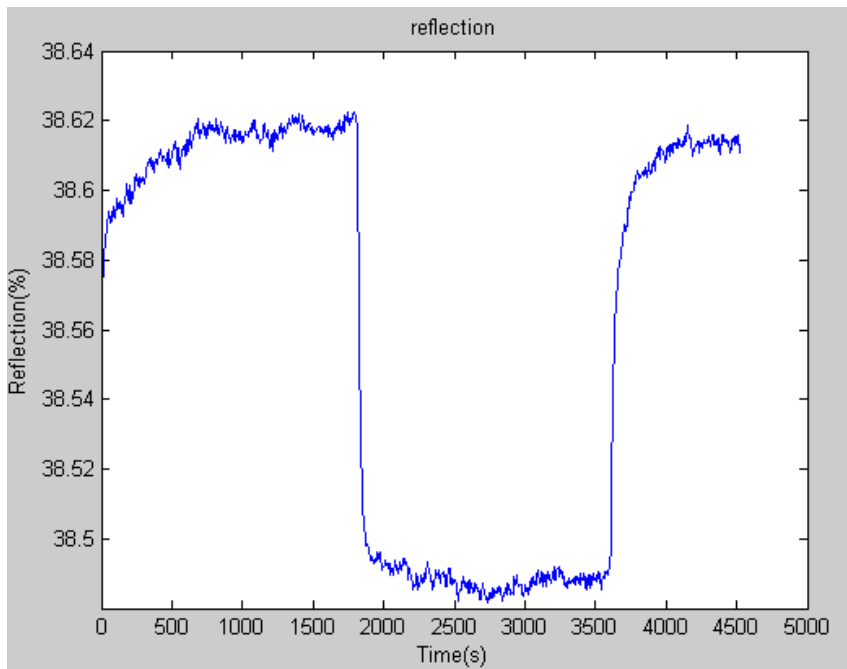


Figure 11

When one is discussing the response time of H<sub>2</sub> sensor, one is always interested in the following:

- Time it takes to respond to H<sub>2</sub> – this is the time that our sensors achieve a stable reflection value upon introduction of H<sub>2</sub> gas at a particular concentration. For our sensors, it is approximately 100 s.
- Time it takes to recover upon H<sub>2</sub> purge – this is the time that our sensors take to recover to its pre-exposure reflection values upon elimination of H<sub>2</sub> from the setup. For our sensors, it is approximately 500 s.

The response times are not competitive with both the lowest achievable time discussed in the literature review section and that of cheaply available commercial sensors. We purchased a commercial resistance-based H<sub>2</sub> sensor for a few dollars that is capable of response times of a few seconds.

Given the slow response time of our optical sensor, another experiment was done with the purchased electrical sensor to monitor the flow of H<sub>2</sub> in the gas flow setup. In that experiment, it was found that H<sub>2</sub> concentration in our setup was at its desired value within a matter of seconds. On the other hand, it takes a few minutes to rid our setup of H<sub>2</sub>. This suggests a possible explanation for the relatively slow recovery times shown in all the reflection graphs in this thesis – gas flow configuration problems. More work needs to be done to speed up the process of H<sub>2</sub> purges to be able to accurately quantify the response time of our optical sensor.

### **3.2.5 Recoverability and the Effects of Annealing**

As discussed in the literature review, the phase change effects in Pd sensors are a potential hindrance to our sensors. We also discussed annealing as a possible solution to this problem.

A 1550 nm light source was used to monitor the response of a sensor to 1.3% H<sub>2</sub>. The sensor has not undergone annealing. The results are shown in Figure 12.

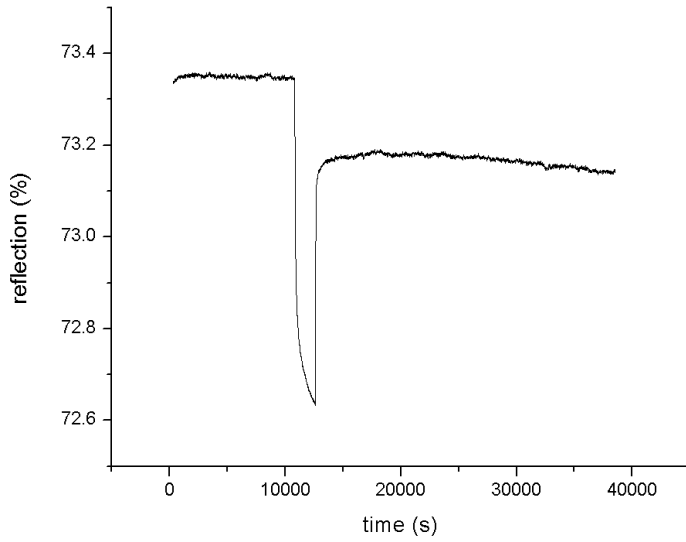


Figure 12

The same light source is used to monitor an annealed sample. This time, various gas concentrations are attempted. The results are shown in Figure 13.

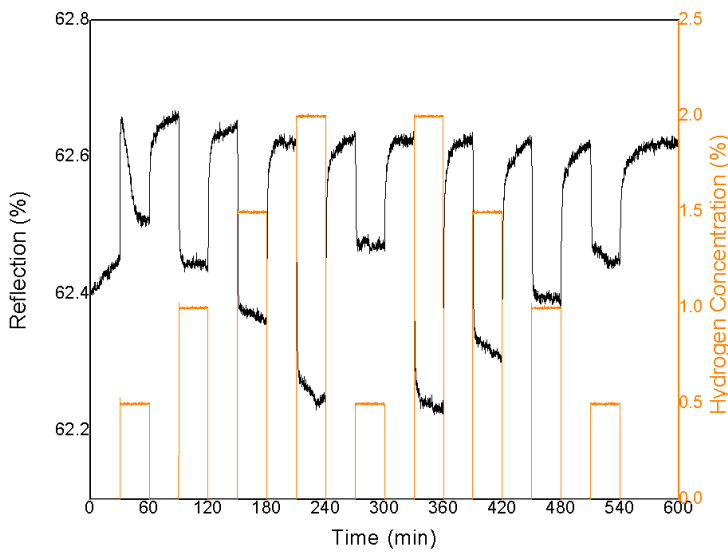


Figure 13

The unannealed sample does not show evidence of complete recovery in a purge time of 25000 s, or about 7 hours while the annealed sample does recover in a matter of minutes for concentrations as high

as 2%. Therefore, we have verified that the process of annealing did address the problem of recoverability caused by the phase change.

### **3.2.6 Deterioration of samples**

We have monitored various samples across long periods of time and have concluded that their sensitivity deteriorates over a period of about half a year, even when stored in an N<sub>2</sub> gas chamber. More effective ways of storing samples is needed in the future.

## 4. Conclusion

Our sensors are competitive in the areas of limit of detection and recoverability, but can be improved upon in the area of response time. As a whole, this project was successful in showing that the Pd Fabry-Perot structure is a viable one for H<sub>2</sub> sensing, even though much more work needs to be done for it to be practical.

### 4.1 Future Work

In addition to various measures proposed in sections 2 and 3, improvements can be made in the following areas:

- Air Pressure Monitoring
- Deposition Conditions

#### 4.1.1 Air Pressure Monitoring

Currently, we do not have a way of monitoring the air pressure surrounding our samples. On the other hand, it is widely known [3] that air pressure is an important factor in the chemical makeup of PdH, which causes changes in refractive indices in the first place.

#### 4.1.2 Deposition Conditions

We have yet to identify the ideal deposition conditions for our samples. Although there was evidence that a slower Pd deposition rate leads to better sample quality, this result was not reproduced for later samples. Also, about 25% of our samples do not respond to H<sub>2</sub> at all. This hints at a certain mistake that we have made during fabrication process that we have yet to narrow down. We can solve this problem by monitoring the fabrication process more closely in the future.

## References

- [1] M. Raval, S. McKeown, A. Arbabi, and L. Goddard, "Palladium Based Fabry-Pérot Etalons for Hydrogen Sensing," in *Imaging and Applied Optics Technical Papers*, OSA Technical Digest (online) (Optical Society of America, 2012), paper STh2B.5.
- [2] S. McKeown and L. L. Goddard, "Hydrogen Detection Using a Single Palladium Nano-aperture on a Fiber Tip," Chapter 15 in *Lab on Fiber Technology*, A. Cusano, M. Consales, A. Crescitelli, A. Ricciardi, editors. Springer, in press.
- [3] S. F. Silva, L. Coelho, O. Frazão, J. L. Santos, and F. X. Malcata, "A Review of Palladium-Based Fiber-Optic Sensors for Molecular Hydrogen Detection." *Sensors Journal*, IEEE **12**, 93–102 (2012).
- [4] T. Hübert, L. Boon-Brett, G. Black, and U. Banach, "Hydrogen sensors – A review." *Sensors and Actuators B: Chemical* **157**, 329 (2011).
- [5] J.H. Song, W. Lu, Operation of Pt/AlGa<sub>N</sub>/Ga<sub>N</sub>-heterojunction field-effect transistor hydrogen sensors with low detection limit and high sensitivity, *IEEE Electron Device Lett.* 29 (2008) 1193–1195.
- [6] T. Xu, M. Zach, Z. Xiao, D. Rosenmann, U. Welp, W. Kwok and G. Crabtree "Self-assembled monolayer-enhanced hydrogen sensing with ultrathin palladium films", *Appl. Phys. Lett.*, vol. 86, pp.203104-1 -203104-3 2005
- [7] Zhao, Z., and M. A. Carpenter. "Annealing Enhanced Hydrogen Absorption In Nanocrystalline Pd<sup>δ</sup>•Au Sensing Films." *Journal of Applied Physics* 97.12 (2005): 124301. Print.
- J.H. Song, W. Lu, Operation of Pt/AlGa<sub>N</sub>/Ga<sub>N</sub>-heterojunction field-effect transistor hydrogen sensors with low detection limit and high sensitivity, *IEEE Electron Device Lett.* 29 (2008) 1193–1195.
- [8] Instruction Manual, 1660 Series Standard Gas Flow Controllers and Meters (2006). *UNIT MFC 1660*. Celerity, Inc Allen, Tx. Urbana, IL.
- [9] Instruction Manual, Smart-Trak Series 100 Mass Flow Meters and Controllers (2009). *Smart-Trak 100*. Sierra Instruments, Monterey, CA. Urbana, IL.